REVISTA DESAFIOS
ISSN: 2359-3652
V.12, n.4, julho/2025 - DOI: 10.20873/2025_jul_17225

DETERMINAÇÃO DA QUANTIDADE DE ADIÇÃO DE MICROSSÍLICA E DA RELAÇÃO ÁGUA/AGLOMERANTE EM CUAD ATRAVÉS DO MÉTODO DO EMPACOTAMENTO ÚMIDO

THE DETERMINATION OF THE CONTENT OF ADDITION OF SILICA FUME AND THE RELATIONSHIP OF WATER/BINDERS IN UHPC THROUGH THE WET PACKGING METHOD

DETERMINACIÓN DE LA CANTIDAD DE ADICIÓN DE MICROSÍLICOS Y LA RELACIÓN AGUA/AGRANTE EN UHPC MEDIANTE EL MÉTODO DE ENVASADO HÚMEDO.

Alessandra Tourinho Maia:

Doutora em Engenharia Civil pelo Programa de Pós-graduação em engenharia civil. Universidade Tecnológica Federal do Paraná (UTFPR). E-mail: alessandra.tourinho@gmail.com | Orcid.org/: 0000-0003-2168-4301

Elizamary Otto Ferreira:

Mestre em Engenharia Civil pelo Programa de Pós-graduação em engenharia civil. Universidade Tecnológica Federal do Paraná (UTFPR). E-mail: elizamaryotto@gmail.com | Orcid.org/0000-0002-2262-7424

Wellington Mazer:

Professor Doutor do Departamento Acadêmico de Construção Civil. Universidade Tecnológica Federal do Paraná (UTFPR). E-mail: wmazer@utfpr.edu,br | Orcid.org/0000-0002-9941-999X

V.12, n.4, julho/2025. ISSN n° 2359-3652

REVISTA DESAFIOS ISSN: 2359-3652

ABSTRACT:

The determination of the optimum amount of constituents, for UHPC production still needs studies, because in many cases this definition is empirical. This work aims to present a methodology for determining the amount of silica fume and to establish a water/binder ratio based on laboratory tests. To define the quantity of constituents necessary for the formation of the paste, the wet packaging method was used and the concentration of solids, the volume of voids and the excess of water were determined. The results indicated that the adopted methodology is adequate, leading to commonly used values, in the present study the optimum quantity of silica fume was 25% associated with a water/binder ratio of 0.18.

KEYWORDS: wet packing method, UHPC, binder content, silica fume, water/binder ratio, concentration of solids, volume of voids, excess of water, laboratory tests, mix methodology.

RESUMO:

A determinação da quantidade ideal de constituintes para a produção de CUAD ainda necessita de estudos, pois em muitos casos essa definição é empírica. Este trabalho tem como objetivo apresentar uma metodologia para determinação da quantidade de sílica ativa e estabelecer uma relação água/aglomerante com base em ensaios de laboratório. Para definir a quantidade de constituintes necessária à formação da pasta, utilizou-se o método do empacotamento úmido e determinou-se a concentração de sólidos, o volume de vazios e o excesso de água. Os resultados indicaram que a metodologia adotada é adequada, levando a valores comumente utilizados, sendo que no presente estudo a quatidade ótima de sílica ativa foi de 25% associada a uma relação água/aglomerante de 0,18.

PALAVRAS CHAVE: *método de embalagem úmida, UHPC, teor de ligante, sílica ativa, relação água/aglutinante, concentração de sólidos, volume de vazios, excesso de água, testes de laboratório, metodologia de mistura.*

RESUMEN:

La determinación de la cantidad óptima de constituyentes para la producción de UHPC aún requiere estudios, ya que en muchos casos esta definición es empírica. Este trabajo tiene como objetivo presentar una metodología para determinar la cantidad de humo de sílice y establecer una relación agua/ligante en base a pruebas de laboratorio. Para definir la cantidad de constituyentes necesarios para la formación de la pasta se utilizó el método de envasado húmedo y se determinó la concentración de sólidos, el volumen de vacíos y el exceso de agua. Los resultados indicaron que la metodología adoptada es adecuada, conduciendo a valores comúnmente utilizados, En el presente estudio la cantidad óptima de humo de sílice fue del 25% asociada a una relación agua/aglutinante de 0,18.

Palabras clave: *Método de empaque húmedo, UHPC, cantidad de aglomerante, humo de sílice, relación agua/ligante, concentración de sólidos, volumen de vacios, excesso de agua, pruebas de laboratório, metodologia de mistura.*

INTRODUCTION

Despite being widely studied, an established dosage procedure for Ultra High Performance Concrete (UHPC) has not yet been presented, and the quantification of its constituents, in many cases, is empirical. In order to make this determination more rational, this work presents a methodology for determining the amount of silica fume and water in the mixture using the wet packaging method proposed by Wong and Kwan (2008).

Many works on UHPC are developed from different dosages, becoming difficult to determine the best amount of its constituents. Table 1 shows a compilation of 60 publications researched between 1995 and 2021, where some parameters observed in the UHPC dosage are indicated, namely: cement consumption (kg/m³); percentage of silica fume in relation to cement mass; water/binder ratio; percentage of quartz powder in relation to cement mass and mass paste content.

Table 1 - Compilation of parameters for different UHPC features

Reference	C	SF	w/b	QP	P
Khaksefidi, S., Ghalehnovi, M., de Brito, J. (2021).	670	30%	0,20	0,42	44%
Sohail, M. G., Kahraman, R., Al Nuaimi, N., Gencturk, B., Alnahhal, W. (2021).	820	23%	0,15		56%
Dong, S.; Wang, Y.; Ashour, A.; Han, B.; Ou, J. (2021)	620	30%	0,24		56%
Liu, J.; Lai, Z.; Chen, B., Xu, S. (2020).	833	30%	0,18		56%
Jung, M., Park, M., Hong, S., Moon,J. (2020).		25%	0,24	0,35	51%
Jiao, Y., Zhang,Y., Guo, M., Zhang, L., Ning, H., Liu,S. (2020).	850	23%	0,15	0,39	49%
Dingqiang, F., Rui, Y., Zhonghe, S., Chunfeng, W., Jinnan, W., Qiqi,S. (2020).	500	25%	0,28		36%
Bae, Y., Pyo,S. (2020).		18%	0,22	14%	43%
Hung, C., Chen, Y., Yen, C. (2020).		22%	0,14	39%	66%
Qu, S., Zhang, Y., Zhu, Y., Huang, L., Qiu, M., Shao, X. (2020).		20%	0,18	20%	53%
Reddy, G.G.K., Ramadoss, P (2020).	800	25%	0,25	30%	50%

REVISTA DESAFIOS ISSN: 2359-3652

Zhu, Y., Zhang,Y., Hussein, H.H., Liu, H., Chen,G. (2020).	771	20%	0,18	20%	54%
Wang, Z., Yan, J., Lin, Y., Fan, F., Yang, F. (2020).	886	25%	0,16	60%	57%
Xu, S., Wu, P., Wu, C. (2020).	750	55%	0,21		58%
Qian, D., Yu, R., Shui, Z., Sun, Y., Jiang, C., Zhou, F., Ding, M., Tong, X., He, Y. (2020).	400	50%	0,18		53%
Gurusideswar, S., Shukla, A., Jonnalagadda, K.N., Nanthagopalan, P. (2020).	1100	20%	0,19	9%	70%
Qiu, M., Zhang, Y., Qu, S., Zhu, Y., Shao, X. (2020).		20%	0,18	20%	53%
Li. P.P.; Brouwers H.J.H., Chen, W. Yu, Q. (2020)	1071	11%	0,17		62%
Kalthoff, M., Raupach, M. (2020).	832	16%	0,19	45%	48%
Zhang, Y., Zhu, Y., Qu, S., Kumar, A., Shao,X. (2020).		20%	0,18	20%	53%
Yan, J., Chen, A., Wang, T. (2020).		25%	0,23	30%	51%
Zhang, X., Li, X., Liu, R., Hao, C., Cao, Z. (2020).	875	29%	0,17		59%
Zhang, Y., Zhu, Y., Qu, S., Kumar, A., Shao, X., Fan, D., Chen, Z., Cai, J., Li, X., He, Y. (2020).	780	25%	0,17		56%
Cai, X., Taerwe, L.R. Yuan, Y. (2020).		30%	0,20		57%
Zhang, Y., Cai, S., Zhu, Y., Fan, L., Shao, X. (2020).	771	20%	0,18	20%	54%
Jung, M., Lee, Y., Hong, S., Moon, J. (2020).		25%	0,23	35%	51%
Tong, L., Chen, L., Wen, M., Xu, C. (2020).		30%	0,20		57%
Zhang, Y., Zhang, C., Zhu, Y., Cao, J., Shao, X. (2020).	771	20%	0,18	20%	53%
Li, X., Li, J., Lu, Z, Hou, L., Chen. J. (2020).	493	16%	0,20		37%
Shen, P., Zheng, H., Xuan, D., Lu, J., Poon, C.S. (2020)	640	28%	0,22		49%
Wang, X., Yu, R., Song, Q., Shui, Z., Liu, Z., Wu, S., Hou, D. (2019).	400	25%	0,18		50%

Haile, B.F.; Jin, D.W.; Yang, B.; Park, S.; Lee, H.K. (2019).		27%	0,23	35%	51%
Zdeb (2019).	903	20%	0,20	34%	56%
Kim, J., Yoo, D. (2019).	789	25%	0,20		51%
Song, Q., Yu, R., Shui, Z., Rao, S., Wang, X., Sun, M., Jiang, C. (2018).	750	19%	0,17		56%
Li, P.P.; Yu, K.L.; Brouwers, H.J.H. (2018).	675	7%	0,20		43%
Pyo, S., Kim, H.K., Lee, B.Y. (2017).		18%	0,22	14%	47%
Aoude, H., Dagenais, F. P., Burrell, R. P., Saatcioglu, M. (2015).	917	25%	0,18		48%
Wille, K., Boisvert-Cotulio, C. (2015).	778	25%	0,23	25%	50%
Alkaysi, M., El-Tawil, S. (2015).	775	25%	0,17		48%
Yao, D., Jia, J., Wu, F., Yu, F. (2014).	420	15%	0,20		30%
Mullen, C. (2013).	710	33%	0,17		47%
Willey, J. (2013).	786	33%	0,22		48%
Willey, J. (2013).	712	32%	0,13		46%
Azad, H. (2013).	900	25%	0,15		56%
Graybeal, B. A., Russell, H. G. (2013).	712	18%	0,13		46%
Wang, C., Yang, C., Liu, F., Wan, C., Pu, X. (2012).	500	10%	0,18		32%
Deeb, R., Ghanbari, A., Karihaloo, B. L. (2012).	544	40%	0,17		57%
Wang, C.,Yang, C., Liu, F., Wan, C., Pu, X (2012).	450	20%	0,15	40%	33%
Akhnoukh, A. K., Xie, H. (2010).	664	21%	0,14		47%
El-Dieb, A. S. (2009).	900	18%	0,19		55%
Yang, S. L., Millard, S. G., Soutsos, M. N., Barnett, S. J., Le, T. T. (2009).	657	18%	0,14		57%
Yunsheng, Z., Wei, S., Sifeng, l., Chujie, J., Jianzhong, L.		25%	0,15		47%

(2008).					
Habel, K., Gauvreau, P. (2008).	967	25%	0,20		68%
Habel *et al.* (2006).	1050	26%	0,15		67%
Ma e Dietz (2002).	609	30%	0,15	43%	37%
Ma e Dietz (2002).	665	30%	0,21	32%	44%
Reda, M. M., Shrive, N. G., Gillott, J. E. (1999).	1010	29%	0,18		67%
Richard e Cheyrezy (1995).	1033	25%	0,13		36%
Richard e Cheyrezy (1995).	959	25%	0,14		56%

Note: C = consumption of cement (kg/m³); SF = percentage of silica fume on the cement mass; w/b = water/binder ratio; QP = percentage of quartz powder on the cement mass; P = mass paste content.

Data analysis shows that the silica fume content adopted by the researchers varies in the range of 7 to 55%, with 25% being the most repeated content, as can be seen in Figure 1. The second most used content is 20%, and, thirdly, the 30% content.

Figure *1* - Silica Fume rate in UHPC.

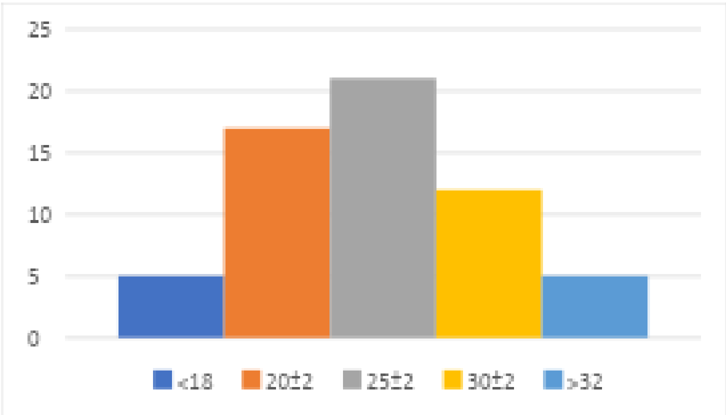

Source: made by authors

According to Richard and Cheyrezy (1995), normally the most used silica/cement ratio is 0.25. This value is close to the dosage necessary to consume the calcium hydroxide resulting from the total hydration of the cement. However, due to the low amount of water used, hydration in the UHPC is incomplete and the amount of available silica is higher than that required by the pozzolans reaction, with the surplus then contributing to the increase in the matrix packing density (MA and DIETZ, 2002).

One method of determining the optimum amount of silica fume in relation to the cement mass is through the wet packing method, proposed by Wong and Kwan (2008).

This method is based on the production of pastes with different water / binder ratios, which vary from insufficient to more than enough to fill the voids between the solid particles, followed by determining the mass of a previously known volume of the pastes produced. From these results, the solids concentration (∅) and the void index (μ) are calculated. There is a water/binder ratio (w/b) corresponding to the maximum concentration of solids, which occurs when the particles are strongly compacted together (KWAN and CHEN, 2012).

For the determination of the solids concentration (∅) and the voids index (μ), the volume of solids in cementitious materials (V_c) and the volume of water (V_w) need to be calculated using Equations 1 and 2:

$$V_c = \frac{M}{\rho_w \mu_w + \rho_\tau R_\tau + \rho_\varphi R_\varphi + \rho_\omega R_\omega} \quad (1)$$

$$V_w = \mu_w . V_c \quad (2)$$

Where: V_c – volume of solid materials; M - mass of the paste; ρ_w – water density; ρ_i – density of solids; R_i - volumetric ratio of the solids; μ_w – water⁄solids ratio by volume.

Having established these values, the concentration of solids (∅) is given by Equation 3 and the voids index (μ) is determined by means of Equation 4. The concentration of solids can be defined as the relationship between the volume of solid materials and the volume of the paste, while the void index is the relationship between the void volume and the volume of solid materials (WONG and KWAN, 2008).

$$\emptyset = \frac{V_c}{V} \quad (3)$$

$$\mu = \frac{(V - V_c)}{V_c} \quad (4)$$

Where: V– volume of the container.

The behavior of the void index and the concentration of solids as a function of the variation of the water/binder ratio can be demonstrated graphically. As can be seen, the concentration of solids initially increases with the increase of the water/binder ratio and then starts to decrease as the amount of water added is more than enough to fill the existing voids (KWAN and CHEN, 2012; WANG et al., 2019).

When the w/b ratio is high, the void rate is also high, indicating that the particles are further apart from each other due to the presence of the water film, forming a suspension with a low concentration of solids. As the water/binder ratio decreases, there is a change in the inflection of the two curves, indicating that the concentration of solids tends to reach its maximum point and the void index, the minimum point. If the w/b ratio is reduced from this point on, the solids concentration will also decrease. This behavior indicates that the water layer around the grains is not continuous and the water is concentrating at the points of contact between the particles, and, due to the surface tension, moving them away and causing a high trap of air in the paste. In this scenario, there is no longer enough water to wet the entire surface of the particles in the mixture (KWAN and WONG, 2008; KLEIN et al., 2016 KWAN and WONG, 2008a; KWAN and CHEN, 2012).

According to Kwan and Chen (2012), the excess water (w) that represents the amount of excess water in the paste in relation to the volume of cementitious materials (V_c needed to fill the voids between the particles, can be calculated as (Equation 5):

$$\mu'_w = \mu_w - \mu \qquad (5)$$

Where: μ_w – water/solids ratio by volume; μ - voids volume.

The negative results of μ'_w indicate that the amount of water added to the pulp is less than the demand, that is, it is not enough to fill the voids between the grains of the pulp, leading to the trapping of air inside it, which turn will induce capillary suction, making the paste drier and less workable. The values in the positive range indicate that the available water is more than enough to fill the existing voids and its excess, resulting from the condition of saturation of the paste, formed films on the surface of the particles that will serve to lubricate the mixture, resulting in different rates fluidity for the different combinations (KWAN and WONG, 2008; WONG and KWAN, 2008a; KWAN and CHEN, 2012; GHASEMI et al., 2019).

The excess water (μ'_w) can also be divided into two parts: that which is essential to promote the onset of fluidity and the amount necessary to reach a certain level of fluidity. The start of the fluidity of the paste is related to the state in which the voids between the particles are completely filled and an additional film of water moistens the surface of the grains, separating them and reducing the friction between the particles. Any increase in water beyond this minimum amount will contribute to the separation of the particles and the consequent increase in the fluidity of the paste (FUNG and KWAN, 2010; KWAN and CHEN, 2012; KWAN and LI, 2012; KLEIN et al., 2016; GHASEMI et al., 2019).

This phenomenon can be observed through the water film thickness (WFT) and is directly related to the specific surface of the grains (A_{CM}) and the packing density of the matrix and can be considered the factor of greater importance in the fluidity and rheology of the paste, mortar and concrete (FUNG and KWAN, 2010; KWAN and CHEN, 2012; KWAN et al, 2012; KLEIN et al., 2016; GHASEMI et al., 2019).

The specific surface of the set of cementitious materials (A_{CM}) per volume unit (m²/m³) is given by Equation 6:

$$A_{CM} = A_\tau R_\tau + A_\varphi R_\varphi + A_\omega R_\omega \qquad (6)$$

Where: A_i– specific surface of the solids; R_i– volumetric ratio of solids.

From the values of A_{CM} and μ'_w, the average thickness of the water film surrounding the particles (WFT) can be calculated as (Equation 7):

$$WFT = \frac{\mu'_w}{A_{CM}} \qquad (7)$$

The relationship between these parameters shows that excess water forms a film on the surface of the particles and the thickness of this film is directly proportional to μ'_w, and inversely proportional to the specific surface of cementitious materials (A_{CM}). The negative water film thickness values indicate that the added water is not enough to fill the empty spaces between the particles, leading to air trapping in the paste (KWAN and WONG, 2008; KWAN and CHEN, 2012).

The addition of silica fume or other fine materials has two main effects on the fluidity of the paste. The first (packaging theory) is related to the high fineness of the particles that will fill the empty spaces between the cement grains, thus increasing the packing density of the mixture and, consequently, the excess water portion (μ'_w) available to lubricate the paste and promote fluidity, or even, for a given fluidity allows the adoption of a lower water/binder ratio, which brings benefits in terms of mechanical resistance and durability (WONG and KWAN, 2008; FUNG and KWAN, 2010; LI and KWAN, 2013; KLEIN et al., 2016).

On the other hand, due to their high fineness, these materials will promote a significant increase in the specific surface of the set (A_{CM}) and, therefore, for the same amount of excess water, the thickness of the water film (WFT) that covers the particles will decrease, as will the fluidity of the paste (water layer theory). Therefore, it can be concluded that the increase in the packing density and the specific surface promote opposite effects on the fluidity of the paste, which can be positive or negative, depending on the magnitude of each one of them (WONG and KWAN, 2008; FUNG and KWAN, 2010; KLEIN et al., 2016).

For Fennis (2011) these two theories are supported by the presence of superplasticizer additives, since in mixtures without the action of steric repulsion promoted by super plasticizers, particle agglomeration can occur, which fail to fill the empty spaces, reducing the availability of excess water.

MATERIALS AND METHODS

MATERIAL SELECTION AND CHARACTERIZATION

For the development of this research, the use of Portland cement with high initial resistance, silica fumes and superplasticizer additive was specified. The characteristics of these materials, commercially available in the national territory, are presented below.

Mineral admixture

The silica fume used as a pozzolan addition is a non-densified material with a specific mass of 2,220 kg/m³, a SiO_2 content greater than 90%, a specific surface (BET) of 19,000 m²/kg and spherical particles with a diameter of 0.20 μm in diameter. Medium.

Table 2 shows the material composition determined by means of the X-ray fluorescence spectrophotometer, brand Shimadzu, model EDX-720 / 800HS.

Table 2 - Composition of silica fume

Oxid	Content (%)
SiO_2	93,02
K_2O	1,90
Fe_2O_3	1,65
Al_2O_3	1,22
SO_3	0,98
Na_2O	0,89
CaO	0,31

Source: Supplier (2020)

Binder

In this research, the binder used was Portland cement with high initial strength (CP V-ARI). According to the test report issued by the manufacturer, the material contains up to 10% limestone filler, has a specific mass of 3,090 kg/m³, a specific surface of 4,363 m²/kg, an average compressive strength of 46.3 MPa at seven days and 56.1 MPa at 28 days of age. Table 3 summarizes the cement composition according to the manufacturer's information.

Table 3 - Cement composition

Oxid	Content (%)
SiO_2	19,02
Fe_2O_3	2,80
Al_2O_3	4,28
SO_3	2,68
MgO	2,90
CaO	62,72

Source: Supplier (2020)

The main physical and chemical parameters of cement are shown in Table *4*. According to the manufacturer, the material meets the specifications of NBR 16697 - Portland Cement - Requirements (ABNT, 2018).

Table 4 - Physical and chemical parameters of cement

Parameter	Value
Stick start time (min.)	175
Loss to fire (%)	3,62
Insoluble residue (%)	0,82
Free CaO (%)	0,97

Source: Supplier (2020)

Chemical Admixture

Due to the low water/binder ratio characteristic of ultra high performance concretes, we opted for the use of a polycarboxylate based superplasticizer chemical admixture. According to the manufacturer, this product has a density of 1,095 kg/m³ and a solids concentration of 47%.

TESTS FOR DETERMINATION OF SILICA FUME CONTENT

The definition of the silica fume cement ratio is fundamental to achieve the minimum porosity of the matrix. For the purpose of this experiment, the contents of 10, 15, 20, 25, 30 and 35% of silica in relation to the cement mass were selected. The water/binder ratio, in mass, ranged from 0.12 to 0.22, in 0.02 increments. These limits were established based on the compilation of related works presented in Table I.

The material mixing procedures followed a sequence similar to that proposed by Wong and Kwan (2008). The cementitious materials were dry pre-mixed. All the water was added to the vat with 50% of the cementitious materials and 20% of the superplasticizer additive. Mixing was carried out at slow speed for a period of two minutes and for another minute at fast speed.

The remaining 50% of the cementitious materials were divided into four equal parts, as well as the remaining additive. Each portion was added to the vat and mixed for two minutes, always at a slow speed in order to attenuate the incorporation of air.

After the production stage, the paste was poured into a metallic cylindrical container of volume 0.394 dm³. After filling, the container was leveled with a metal ruler in order to remove excess material and the mass of the set (container + paste) was determined with the aid of a precision electronic scale.

The parameters solids concentration (∅) and void volume (μ) resulting from the test were determined using Equations 1 to 4. According to the method proposed by Wong and Kwan (2008), varying the water / binder ratio in volume within the analyzed range, the paste that results in the lowest void volume and the highest concentration of solids is the one that has the highest packing density.

DETERMINATION OF THE WATER/BINDER RATIO

The water/binder ratio (w/b) was established from the wet packaging test described above. For this purpose, it was determined, using Equation E, the excess water present in the paste (μ'_w) for each of the different mass w/b ratios used in the test. The water/binder ratio of each silica content was defined as that corresponding to the value of μ'_w immediately greater than or equal to zero. It is also noteworthy that the lower the value of μ'_w, the lower the fluidity of the paste.

RESULTS AND DISCUSSION

DETERMINING THE SILICA FUME CONTENT

In Figure 2, the results of the wet packaging test are presented, according to the methodology presented by Wong and Kwan (2008), with the contents of 10%, 15%, 20%, 25%, 30% and 35% being illustrated in figures A, B, C, D, E and F, respectively.

Figure 2 - Wet packaging curves.

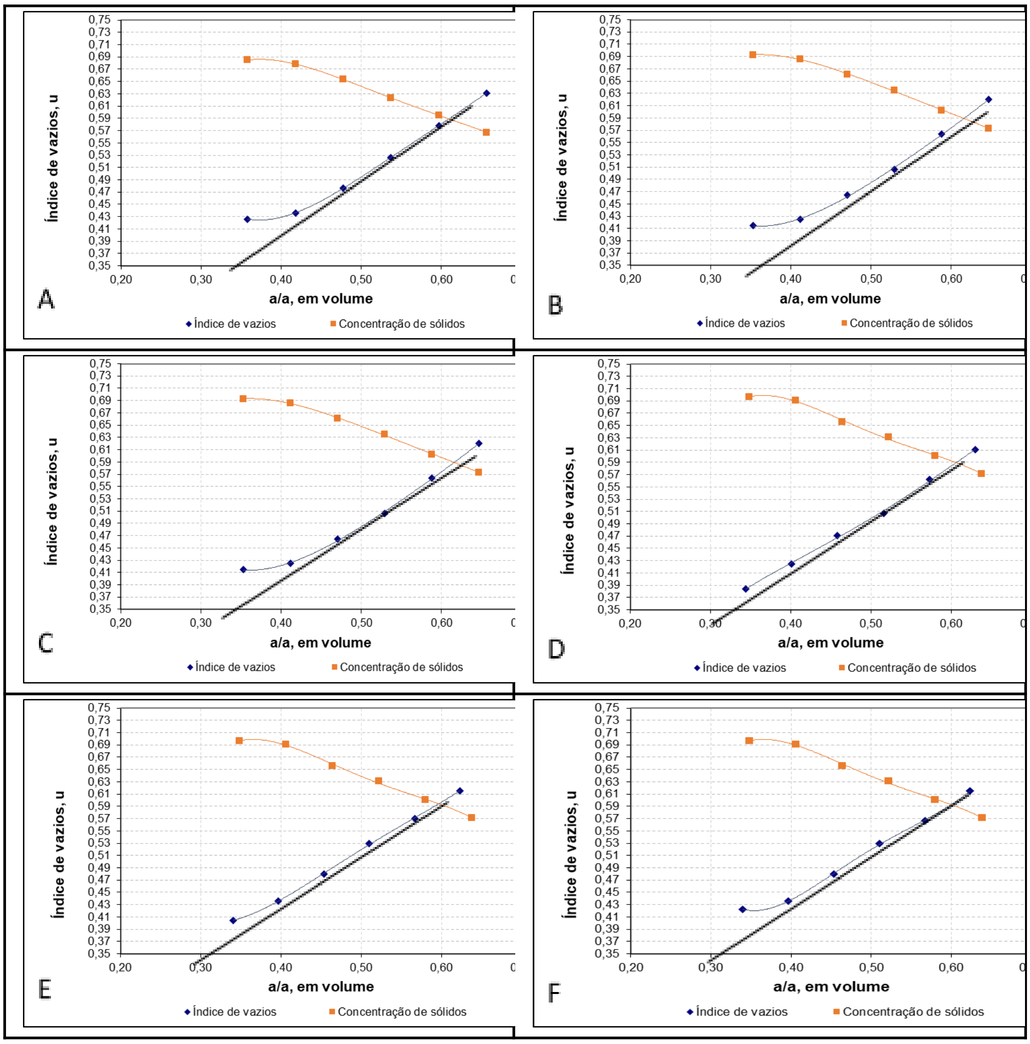

Source: made by authors

According to Wong and Kwan (2008) when the void rate is equal to the water rate ($\mu = \mu_w$) there is a condition that the amount of air is zero ($\varepsilon_a = 0$) and this can be determined at from a tangent drawn to the ascending section of the curve voids volume x w/b ratio, the voids index being determined by the horizontal distance between the two curves. It is possible to observe in Figure 2 that for the lowest values of addition of silica fume (10% and 15%) this phenomenon occurs for w/b ratio close to 0.40, for the addition levels of 30% and 35%, similar behavior occurs for w/b ratio close to 0.35 and the lowest value of w/b ratio was observed for the 25% active silica content, indicating that the increase in the addition content produces a reduction in the voids index of the mixture and after a certain limit an increase of this index occurs again. This can be explained by the packaging that the active silica promotes next to the cement due to its lower diameter followed by the spacing effect caused by the excess of fines.

Similar analysis can be carried out regarding the concentration of solids, which tends to increase with the increase of the content of addition of silica fume up to the limit of 25%, followed by the decrease of its value, corroborating with the theory of improvement of the packaging of particles with the silica fume filling the spaces between the cement grains until the excess fines cause the spacing effect.

Table 5 shows the highest solids concentration values observed in the tests, as well as the respective void volumes and w/b ratio in mass and volume for each content of added silica fume used. Figure 3A shows the graphical representation of the concentration of solids as a function of the addition content by means of an adjusted trend curve. Figure 3B shows the void content as a function of the addition content from an adjusted trend curve.

Table 5 – Results of the wet packaging test for different silica fume contents

Silica fume content on the cement mass (%)	w/b ratio (mass/volume)	Void Volume (μ)	Solids concentration (∅)
10	0.12/0.36	0.4261	0.7012
15	0.12/0.35	0.4143	0.7070
20	0.12/0.35	0.4088	0.7098
25	0.12/0.34	0.3839	0.7226
30	0.12/0.34	0.4223	0.7031
35	0.12/0.34	0.4523	0.7047

Source: made by authors

Figure 3 - Solid concentration and voids index curves

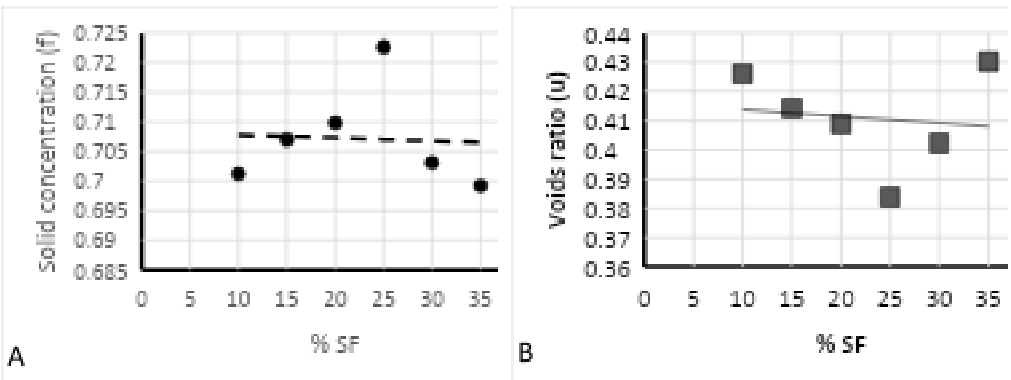

The results obtained indicate that the silica content of 25% is what leads to the highest packing density and the lowest volume of voids within the studied range, and that from this content, the concentration of solids starts to decrease with a consequent increase in voids volume. This result coincides with the values adopted by several researchers (DINGQIANG et al, 2020; REDDY and RAMADOSS, 2020; WANG et al, 2020; WANG et al, 2019; WILLE and BOISVERT-COTULIO, 2015).

REVISTA DESAFIOS ISSN: 2359-3652

Note that for the silica fume content of 10% and 15%, from the water/binder ratio of 0.16, the parameter representing excess water assumes positive values, indicating that, from this point on, water is available to lubricate the grains and promote the fluidity of the paste, and all the authors indicated in Table 1 who used a percentage of silica fume close to these values adopted a w/b ratio greater than 0.16. As the percentage of silica fume increases (20% and 25%), the demand for water also increases and the minimum w/b ratio becomes 0.18 so that there is excess water. In this case, of the 37 authors who used this percentage of silica fume, 23 studies used a ratio w/b equal to or greater than 0.18. For the silica content of 30% and 35%, the pattern is repeated and the excess water available occurs from the water/binder ratio of 0.20, and for this range of silica fume use, eight authors worked with respect w/b equal to or greater than 0.20. The increase in water demand is justified by the high fineness of the silica fume, increasing the specific surface of the grains in the mixture with a consequent increase in the demand for water to wet all grains. The methodology presented is consistent with the values used in most surveys.

JOINT ANALYSIS OF SILICA CONTENT AND W/B RATIO

As the increase in excess water occurs, it is possible to observe a reduction in packing density, as illustrated in Figure 4.

Figure 4 - Packaging density x excess water ratio.

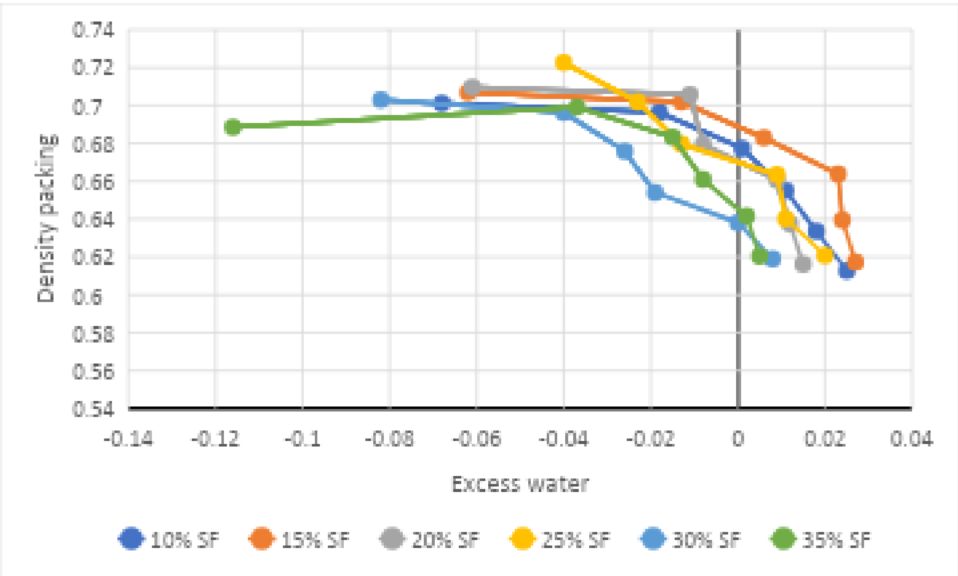

Source: made by authors

To produce UHPC with adequate fluidity for molding, it is necessary that the amount of water is sufficient to lubricate all the grains, that is, the excess water needs to be equal to or greater than zero, even though the packing density of the mixture is reduced. The packing density for mixtures with excess water greater than or equal to zero is shown in Table 6.

Table 6 – Results of the wet packaging test for different silica fume contents

Silica fume content on the cement mass (%)	w/b ratio (mass/volume)	Excess water	Packaging density (Ø)	Increase in w/b ratio (%)	Decreased packing density (%)
10	0.16/0.48	0.001	0.6774	33.33	3.39
15	0.16/0.47	0.006	0.6829	33.33	3.41
20	0.18/0.52	0.009	0.6607	50.00	6.61
25	0.18/0.52	0.009	0.6635	50.00	8.18
30	0.20/0.57	0.000	0.6382	66.67	9.23
35	0.20/0.57	0.002	0.6415	42.79	8.25

Source: made by authors

When analyzing the highest packing density in isolation, it appears that the 25% content of added silica fume leads to the highest packing density, however when considering the minimum amount of water necessary to lubricate all grains, the contents of silica fume of 10% and 15% show the smallest increase in the w/b ratio and the smallest decreases in packing density, in percentage terms.

Through the compilation of dashes for UHPC presented it is possible to observe that the most used silica content is 25%, associated with the w/b ratio of 0.18, showing that the determination of the highest packing density indicates a silica content active suitable for making UHPC with a sufficient amount of water to wet all grains, obtained by determining excess water.

CONCLUSION

A review of UHPC traces was performed to verify the content of silica fume and the most common w/b ratio to outline the parameters of the methodology used to determine the optimal amount of these constituents.

The wet packing technique is suitable for determining the optimum amount of silica fume, indicating the highest packing density for several mixtures. However, it was found that the amount of water that leads to the highest concentration of solids might not be adequate, since there may still be voids in the mixture. To overcome this problem, an analysis of excess water must be carried out, which indicates the minimum amount of water needed to wet all grains and fill all voids.

Finally, it was found that using the wet packaging method, it is possible to determine the optimum content of silica fume by means of the highest concentration of solids, and to choose the w/b ratio by determining the excess water in the mixture.

Acknowledgements

To the Federal Technological University of Paraná (UTFPR), Civil Construction Research Laboratory, Multiuser Center for Materials

Characterization and the Multiuser Laboratory for Chemical Analysis of UTFPR - Curitiba.

References

AKHNOUKH, A. K.; XIE, H. "Welded wire reinforcement versus random steel fibers in precast/prestressed ultra-high performance concrete I-girders **Construction and Building Materials**, 24(11), 2200–2207. 2010.

ALKAYSI, M.; EL-TAWIL, S. Structural response of joints made with generic UHPC. **Proceedings, Structures Congress**, ASCE, Reston,VA, 1435–1445. 2015.

AOUDE, H.; DAGENAIS, F. P.; BURRELL, R. P.; SAATCIOGLU, M. Behavior of ultra-high performance fiber reinforced concrete columns under blast loading Int. **Journal of Impact Engineering**, 80, 185–202.2015. 2015.

AZAD, A. K.; HAKEEM, I. Y. Flexural behavior of hybrid concrete beams reinforced with ultra-high performance concrete bars. **Construction and Building Materials**, 49, 128–133. 2013.

BAE, Y.; PYO, S. Effect of steel fiber content on structural and electrical properties of ultra high performance concrete (UHPC) sleepers, **Engineering Structures**, Vol. 222, 111131, ISSN 0141-0296. 2020.

CAI, X.; TAERWE, L.R.; YUAN, Y. Hysteretic behavior of UHPC beam-column joints after fire exposure, **Fire Safety Journal**, Vol. 117, 102987, ISSN 0379-7112. 2020.

DEEB, R.; GHANBARI, A.; KARIHALOO, B. L. Development of self compacting high and ultra high performance concretes with and without steel fibers. **Cem. Concr. Compos.** 34(2), 185–190. 2012.

DINGQIANG, F.; RUI, Y.; ZHONGHE, S.; CHUNFENG, W.; JINNAN, W.; QIQI, S. A novel approach for developing a green Ultra-High Performance Concrete (UHPC) with advanced particles packing meso-structure. **Construction and Building Materials**, 265, 120339. 2020.

DONG, S.; WANG, Y.; ASHOUR, A.; HAN, B.; OU, J. Uniaxial compressive fatigue behavior of ultra-high performance concrete reinforced with super-fine stainless wires, **International Journal of Fatigue**, Volume 142, 105959, ISSN 0142-1123. 2021.

EL-DIEB, A. S. Mechanical, durability and microstructural characteristics of ultra-high-strength self-compacting concrete incorporating steel fibers. **Mater. Des.**, 30(10), 4286–4292. 2009.

FUNG, W.W.S.; KWAN, A.H.K. Role of water film thickness in rheology of CSF mortar. **Cement & Concrete Composites**. Volume 32, Issue 4, p. 255-264. 2010.

GHASEMI, Y.; EMBORG, M.; CWIRZEN, A. Effect of water film thickness on the flow in conventional mortars and concrete. **Materials and Structures**, 52:62. 2019.

GRAYBEAL, B. A.; RUSSELL, H. G. Ultra-high performance concrete: A state-of-the-art report for the bridge community, **Publication No. *FHWA-HRT-13-060***. 2013.

GURUSIDESWAR, S.; SHUKLA, A.; JONNALAGADDA, K.N.; NANTHAGOPALAN, P. Tensile strength and failure of ultra-high performance concrete (UHPC) composition over a wide range of strain rates, **Construction and Building Materials**, Vol. 258, 119642, ISSN 0950-0618. 2020.

HABEL, K.; VIVIANI, M.; DENARIÉ, E.; BRÜHWILER, E. Development of the mechanical properties of an ultra-high performance fiber reinforced concrete (UHPFRC). **Cement and Concrete Research**., 36(7), 1362–1370. 2006.

HABEL, K.; GAUVREAU, P. Response of ultra-high performance fiber reinforced concrete (UHPFRC) to impact and static loading, **Cement and Concrete Composites**, Vol. 30, Issue 10, p. 938-946, ISSN 0958-9465. 2008.

HAILE, B.F.; JIN, D.W.; YANG, B.; PARK, S.; LEE, H.K. Multi-level homogenization for the prediction of the mechanical properties of ultra-high-performance concrete. **Construction and Building Materials.** Vol. 229, 116797. 2019.

HUNG, C.; CHEN, Y.; YEN, C. Workability, fiber distribution, and mechanical properties of UHPC with hooked end steel macro-fibers, **Construction and Building Materials**. Vol. 260, 119944, ISSN 0950-0618. 2020.

JIAO, Y.; ZHANG, Y.; GUO, M.; ZHANG, L.; NING, H.; LIU, S. Mechanical and fracture properties of ultra-high performance concrete (UHPC) containing waste glass sand as partial replacement material, **Journal of Cleaner Production**, Vol. 277, 123501, ISSN 0959-6526. 2020.

JUNG, M.; PARK, J.; HONG, S.; MOON, J. Electrically cured ultra-high performance concrete (UHPC) embedded with carbon nanotubes for field casting and crack sensing, **Materials & Design,** Vol. 196, 109127, ISSN 0264-1275. 2020.

JUNG, M.; LEE, Y.; HONG, S.; MOON, J. Carbon nanotubes (CNTs) in ultra-high performance concrete (UHPC): Dispersion, mechanical properties, and electromagnetic interference (EMI) shielding effectiveness (SE), **Cement and Concrete Research**, Vol. 131, 106017, ISSN 0008-8846. 2020.

KALTHOFF, M.; RAUPACH, M. Pull-out behavior of threaded anchors in fibred reinforced ordinary concrete and UHPC for machine tool constructions, **Journal of Building Engineering**, 101842, ISSN 2352-7102. 2020.

KHAKSEFIDI, S.; GHALEHNOVI, M.; DE BRITO, J. Bond behavior of high-strength steel rebar's in normal (NSC) and ultra-high performance concrete (UHPC). **Journal of Building Engineering**, 33. 2021.

KIM, J.; YOO, D. Effects of fiber shape and distance on the pullout behavior of steel fibers embedded in ultra-high-performance concrete, **Cement and Concrete Composites**, V. 103, p. 213-223, ISSN 0958-9465. 2019.

KLEIN, N.S.; CAVALARO, S.; AGUADO, A.; SEGURA, I.; TORALLES, B. The wetting water in cement-based materials: Modeling and experimental validation. **Construction and Building Materials**, v.121, p. 34–43. 2016.

KWAN, A.K.H.; CHEN, J.J. Roles of packing density and water film thickness in rheology and strength of cement paste. **Journal of Advanced Concrete Technology**, v. 10, p. 332-344. 2012.

KWAN, A.K.H; LI, L.G.; FUNG, W.W.S. Wet packing of blended fine and coarse aggregate. **Materials and Structures**, 45:817–828. 2012.

LI, P.P.; BROUWERS, H.J.H.; CHEN, W.; YU, O. Optimization and characterization of high-volume limestone powder in sustainable ultra-high performance concrete. **Construction and Building Materials**, 242, 118112. 2020.

LI, P.P.; YU, K.L.; BROUWERS, H.J.H. Effect of coarse basalt aggregates on the properties of Ultra-high Performance Concrete (UHPC) **Construction and Building Materials**, v. 10, p. 649-659. 2018.

LI, X.; LI, J.; LU, Z; HOU, L.; CHEN. J. Preparation and properties of reactive powder concrete by using titanium slag aggregates. **Construction and Building Materials**, v. 234, 117342. 2020.

LIU, J.; LAI, Z.; CHEN, B., XU, S. Experimental behavior and analysis of steel-laminated concrete (RC and UHPC) composite girders. **Engineering Structures**, V. 225, 111240, ISSN 0141-0296. 2020.

MA, J.; DIETZ, J. Ultra High Performance Self-Compacting Concrete. **LACER** N° 7. 2002.

MULLEN, C. **Determining the effect of thermal treatment timing on ultra-high performance concrete beams**. Master's thesis, Michigan Technological Univ., Houghton, MI. 2013.

PYO, S.; KIM, H.; LEE, B.Y. Effects of coarser fine aggregate on tensile properties of ultra high performance concrete. **Cement and Concrete Composites,** v. 84, p. 28-35. 2017.

QU, S.; ZHANG, Y.; ZHU, Y.; HUANG, L.; QIU, M.; SHAO. X. Prediction of tensile response of UHPC with aligned and ZnPh treated steel fibers based on a spatial stochastic process, **Cement and Concrete Research**, v. 136, 106165. 2020.

QIU, M.; ZHANG, Y.; QU, S.; ZHU, Y.; SHAO, X. Effect of reinforcement ratio, fiber orientation, and fiber chemical treatment on the direct tension behavior of rebar-reinforced UHPC, **Construction and Building Materials**, v. 256, 119311, ISSN 0950-0618. 2020.

REDA, M. M.; SHRIVE, N. G.; GILLOTT, J. E. Microstructural investigation of innovative UHPC. **Cement and Concrete Research**, v. 29(3), p. 323–329. 1999.

REDDY, G.G.K.; RAMADOSS, P. Influence of alccofine incorporation on the mechanical behavior of ultra-high performance concrete (UHPC), **Materials Today: Proceedings**, ISSN 2214-785. 2020.

RICHARD, P.; CHEYREZY, M. Composition of reactive power concretes. **Cement and Concrete Research**, v. 25. no. 7, p. 1501-1511. 1995.

SHEN, P.; ZHENG, H.; XUAN, D.; LU, J.; POON, C.S. Feasible use of municipal solid waste incineration bottom ash in ultra-high performance concrete. **Cement and Concrete Composites**, v. 114, 103814. 2020.

SOHAIL, M.G; WANG, B.; RAMAZAN, K.; AL NUAIMI, N.; GENCTURK, B.; ALNAHHAL, W. Durability characteristics of high and ultra-high performance concretes. **Journal of Building Engineering**. v. 33, 101669. 2021.

SONG, Q.; YU, R.; SHUI, Z.; RAO, S.; WANG, X.; SUN, M.; JIANG, C. Steel fibre content and interconnection induced electrochemical corrosion of Ultra-High Performance Fibre Reinforced Concrete (UHPFRC), **Cement and Concrete Composites**, v. 94, p. 191-200, ISSN 0958-9465. 2018.

TONG, L.; CHEN, L.; WEN, M.; XU, C. Static behavior of stud shear connectors in high-strength-steel–UHPC composite beams, **Engineering Structures**, v. 218, 110827, ISSN 0141-0296. 2020.

WANG, Z.; YAN, J.; LIN, Y.; FAN, F.; YANG. Y. Mechanical properties of steel-UHPC-steel slabs under concentrated loads considering composite action, **Engineering Structures**, v. 222, 111095, ISSN 0141-0296. 2020.

WANG, X.; YU, R.; SONG, Q.; SHUI, Z.; LIU, Z.; WU, S.; HOU, D. Optimized design of ultra-high performance concrete (UHPC) with a high wet packing density, **Cement and Concrete Research**, v. 126, 105921, ISSN 0008-8846. 2019.

WILLE, K.; BOISVERT-COTULIO, C. Material efficiency in the design of ultra-high performance concrete, **Construction and Building Materials**, v. 86, p. 33-43, ISSN 0950-0618. 2015.

WILLEY, J. **Use of ultra-high performance concrete to mitigate impact and explosive threats**. Master's thesis, Missouri Univ. of Science and Technology, Rolla, MO. 2013.

WONG, H.H.C.; KWAN, A.K.W. Packing density of cementitious materials: part 1 – measurement using a wet packing method. **Materials and Structures,** v. 41, p. 689 - 701. 2008.

WONG, H.H.C.; KWAN, A.K.W. Packing density of cementitious materials: part 2– packing and flow of OPC + PFA+ CSF. **Materials and Structures,** v. 41, p. 773 - 784. 2008a.

XU, S.; WU, P.; WU, C. Calibration of KCC concrete model for UHPC against low-velocity impact, **International Journal of Impact Engineering**, v. 144, 103648, ISSN 0734-743X. 2020.

YAN, J.; CHEN, A.; WANG, T. Compressive behaviors of steel-UHPC-steel sandwich composite walls using novel EC connectors, **Journal of Constructional Steel Research**, v. 173, 106244, ISSN 0143-974X. 2020.

YANG, S. L.; MILLARD, S. G.; SOUTSOS, M. N.; BARNETT, S. J.; LE, T. T. Influence of aggregate and curing regime on the mechanical properties of ultra-high performance fibre reinforced concrete (UHPFRC). **Construction and Building Materials**, v. 23(6), p. 2291–2298. 2009.

YAO, D.; JIA, J.; WU, F.; YU, F. Shear performance of prestressed ultra high strength concrete encased steel beams. **Construction and Building Materials,** v. 52, p. 194–201. 2014.

YUNSHENG, Z.; WEI, S.; SIFENG, L.; CHUJIE, J.; JIANZHONG, L. Preparation of C200 green reactive powder concrete and its static–dynamic behaviors, **Cement and Concrete Composites**, v. 30, Issue 9, p. 831-838, ISSN 0958-9465. 2008.

ZDEB, T. Effect of vacuum mixing and curing conditions on mechanical properties and porosity of reactive powder concretes. **Construction and Building Materials**, v. 209, p. 326–339. 2019.

ZHANG, X.; LI, X.; LIU, R.; HAO, C.; CAO, Z. Dynamic properties of a steel–UHPC Composite deck with large U-ribs: Experimental measurement and numerical analysis, **Engineering Structures**, v. 213, 110569, ISSN 0141-0296. 2020.

ZHANG, Y.; ZHU, Y.; QU, S.; KUMAR, A.; SHAO, X. Improvement of flexural and tensile strength of layered-casting UHPC with aligned steel fibers. **Construction and Building Materials**, v. 251, 118893, ISSN 0950-0618. 2020.

ZHANG, Y.; ZHU, Y.; QU, S.; KUMAR, A.; SHAO, X.; FAN, D.; CHEN, Z.; CAI, J.; LI, X.; HE, Y. Feasibility analysis of treating recycled rock dust as an environmentally friendly alternative material in Ultra-High Performance Concrete (UHPC), **Journal of Cleaner Production**, v. 258, 120673, ISSN 0959-6526. 2020.

ZHANG, Y.; CAI, S.; ZHU, Y.; FAN, L.; SHAO, X. Flexural responses of steel-UHPC composite beams under hogging moment, **Engineering Structures**, v. 206, 110134, ISSN 0141-0296. 2020.

ZHANG, Y.; ZHANG, C.; ZHU, Y.; CAO, J.; SHAO, X. An experimental study: various influence factors affecting interfacial shear performance of UHPC-NSC, **Construction and Building Materials**, v. 236, 117480, ISSN 0950-0618. 2020.

ZHU, Y.; ZHANG, Y.; HUSSEIN, H.H.; LIU, J.; CHEN, G. Experimental study and theoretical prediction on shrinkage-induced restrained stresses in UHPC-RC composites under normal curing and steam curing, **Cement and Concrete Composites**, v. 110, 103602, ISSN 0958-9465. 2020.